Bond Thickness Effects upon Stresses in Single-Lap Adhesive Joints

I. U. Ojalvo* and H. L. Eidinoff*
Grumman Aerospace Corp., Bethpage, N. Y.

Results of an analytical investigation on the influence of bond thickness upon the stress distribution in single-lap adhesive joints are presented. The present work extends the basic approach for bonded joints, orginally introduced by Goland and Reissner, through use of a more complete shear-strain/displacement equation for the adhesive layer. This refinement was not found to be included in any of the numerous analytical investigations reviewed. As a result of the approach employed, the present work uncovers several interesting phenomena without adding any significant complication to the analysis. Besides modifying some coefficients in the shear stress equations, completely new terms in the differential equation and boundary conditions for bond peel stress are obtained. In addition, a variation of shear stress through the bond thickness, no matter how thin it may be, is analytically predicted only by the present theory. This through-the-bond-thickness variation of shear stress identifies two antisymmetrical adherend-bond interface points at which the shear stresses are highest. The growth of joint failures originating from these points agrees with results obtained from actual experiments.

Nomenclature

A,B,C,D = shear and peel bond stress solution constants
c = half overlap length of joint
E = modulus of elasticity of adherends
E^* = effective modulus of adherends
E_a = effective thickness-stretching stiffness of adhesive
G_a = adhesive shear modulus
h = bond thickness
k = induced edge moment factor
M_i = moment in adherends
M_0 = induced adherend moment at ends of joint
N_i = tensile force in adherends
N_0 = tensile load across joint
Q_a = transverse shear in adhesive
Q_i = transverse shear in adherends
Q_0 = induced shear in adherends at ends of joint
t = adherend thickness
$\bar{u}_i$ = longitudinal displacement at bond-adherend interface
u_a = longitudinal displacement in adhesive
w_a = transverse displacement in adhesive
w_i = transverse displacement in adherends
x = longitudinal coordinate
z = thickness coordinate
α_1 = see Eq. (50)
α_2 = see Eq. (51)
β = bond to adherend thickness ratio [see Eq. (15)]
γ = joint thickness to length ratio [see Eq. (46)]
γ_a = shear strain in adhesive
ξ = joint tensile load to stiffness ratio [see Eq. (37)]
λ = bond shear to adherend stiffness ratio [see Eq. (18)]
ν = Poisson's ratio for adherends
ρ = bond peel to adherend bending stiffness ratio [see Eq. (26)]
σ_a = peel stress in adhesive
σ_i = peel stress at adherend-bond interface
$\bar{\tau}$ = average joint shear stress
τ_i = shear stress at adherend-bond interface
τ_0 = bond shear stress along $z = 0$ (z axis)
$\Delta\tau$ = shear stress increment from τ_0 along bond-adherend interface
$( )^*$ = nondimensional variable [see Eq. (38)]
$( )'$ = derivative with respect to x [prior to Eq. (37)] or x^* [after Eq. (37)]

Subscript

i = adherend 1 or 2

IN their pioneering work on single-lap bonded joints, Goland and Reissner[1] employed an incomplete shear-strain/displacement equation for the adhesive. Their paper, which represents a classic in the field, was published over 30 years ago. Nevertheless, the deficiency in their shear-strain expression has been perpetuated ever since. Therefore, it appears appropriate to correct this feature of their work. The present paper does so, in a manner which does not complicate the analysis to any significant degree, and assesses the effect of this correction.

In addition, the importance of including certain geometric nonlinearity effects, associated with the fact that the transverse joint deflections are of the order of the adherend thicknesses, is highlighted. Many investigators[2-4] have neglected this consideration entirely, in spite of its inclusion by Goland and Reissner[1] who treated it in an approximate manner. This nonlinear beam-tension effect, which produces a significant reduction of stress concentration in the adherends, was refined by Hart-Smith,[5] in a manner which showed considerable insight.

In the research of Grimes, et al.,[2] Dickson, et al.,[3] and Vinson and Renton,[4] thickness stretching and transverse shear in the adherends were included. This made is possible to satisfy the additional condition of zero adhesive shear, at the ends of the joint region, which resulted in prediction of a boundary layer effect. References 2, 5, and 6 also treated plasticity in the adhesive. A number of references have also treated composite and nonidentical adherends. However, none of these complicating effects are included here. Rather, we have chosen to focus entirely on a specific item which has hitherto been neglected, i.e., the influence of bond thickness upon the elastic adhesive stresses. In doing so, we have uncovered several interesting phenomena which are developed in

Received March 18, 1977; revision received Nov. 15, 1977; presented as Paper 770090 at the SAE Annual Meeting, Jan. 1977; released to the American Institute of Aeronautics and Astronautics, Inc.

Index categories: Structural Design; Structural Statics; Structural Composite Materials.

*Structural Mechanics Engineer.

detail. These include corrections to the coefficients of the governing adhesive differential and boundary equations and some new terms in the peel stress equations. In addition, only the present formulation predicts a through-the-thickness variation in shear stress which identifies the most highly stressed regions in the adhesive. These prove to be at particular bond-adherend interface points, at either end of the joint, where actual tests indicate bond failures initiate and propagate through the joint in a predictable manner.

Governing equations and numerical solutions are compared with Goland and Reissner's work and graphical results on the effects of bond thickness are presented. The form of these results helps to identify the significant joint structural parameters and to assess the influence of adhesive thickness upon joint stresses.

Assumptions

Three simplifying assumptions are made which form the basis of the governing theory to be developed. These assumptions are physically justifiable and concern the behavior of the elements which compose the joint.

1) The longitudinal direct stresses in the bond material are negligible when compared with those in the adherends.

2) The adherends deform as classical thin materials in either plane stress or plane strain, i.e., plane sections remain plane and cross sections deform normal to their individual middle surfaces.

3) Longitudinal and transverse deflections in the bond material vary linearly through the adhesive thickness between the adherends.

The preceding assumptions are cited when they are first employed in the ensuing development.

Governing Differential Equations

The coordinate system for the undeformed joint and its geometric parameters are presented in Fig. 1. For simplicity in the ensuing development, we have selected identical adherends. Referring to Fig. 2a, the combined moment and shear equilibrium equations for a typical composite differential element, inside the joint region, are

$$M_1' + M_2' - (N_1' - N_2')(h+t)/2 + (Q_1 + Q_2 + Q_a) = 0 \quad (1)$$

and

$$(Q_1 + Q_2 + Q_a)' = 0 \quad (2)$$

respectively, where primes denote differentiation with respect to x. Use has been made of Assumption 1 in Eq. (1) and Fig. 2a, since the adhesive carries no longitudinal force or moment resultants. However, the same equations for each adherend give (see Fig. 2b)

$$M_1' + Q_1 - \tau_1 (t/2) = 0 \quad (3a)$$

$$M_2' + Q_2 - \tau_2 (t/2) = 0 \quad (3b)$$

and

$$Q_1' - \sigma_1 = 0 \quad (4a)$$

$$Q_2' + \sigma_2 = 0 \quad (4b)$$

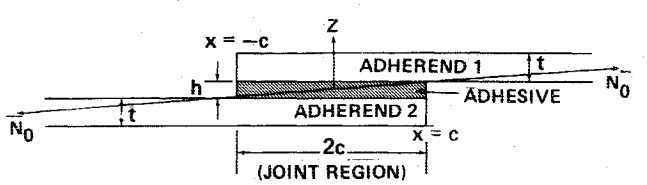

Fig. 1 Geometry of undeformed single-lap adhesive joint.

The horizontal equilibrium equations for each adherend are

$$N_1' - \tau_1 = 0 \quad (5a)$$

and

$$N_2' + \tau_2 = 0 \quad (5b)$$

The force and moment resultants, N_i, Q_i, and M_i $(i=1, 2)$ are internal load intensities per unit width normal to the z-x plane.

Combination of Eqs. (1-3) with Eq. (5) yields an equation which is equivalent to moment equilibrium in the adhesive, i.e.,

$$Q_a = h\tau_0 \quad (6)$$

where τ_0 is defined as the average of the shear stress components τ_1 and τ_2

$$\tau_0 \equiv (\tau_1 + \tau_2)/2 \quad (7)$$

The main difference between the preceding equations and those presented in Refs. 1-5 is that the bond stress reactions, σ_i and τ_i, are permitted to be different on the two adherends. In the ensuing derivation, we shall see that Assumption 3 leads to an equivalence of the peel stresses, σ_i, but not the shear stresses, τ_i $(i=1, 2)$.

Denoting the transverse deflections of the adherends by w_i, both measured positive upward, Assumption 2 yields

$$w_i'' = 12M_i/E^*t^3 \qquad (i=1, 2) \quad (8)$$

where $E^* = E$ for adherends in plane stress and $E/(1-\nu^2)$ for adherends in plane strain.

Based on Assumption 2, the longitudinal strains in the adherends at the bond interfaces are expessed in terms of the

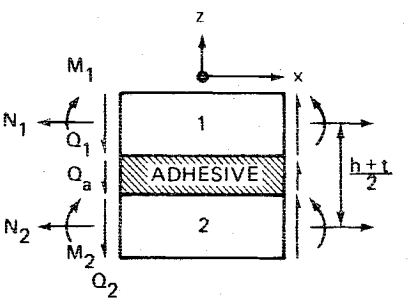

Fig. 2a Typical composite element inside joint region.

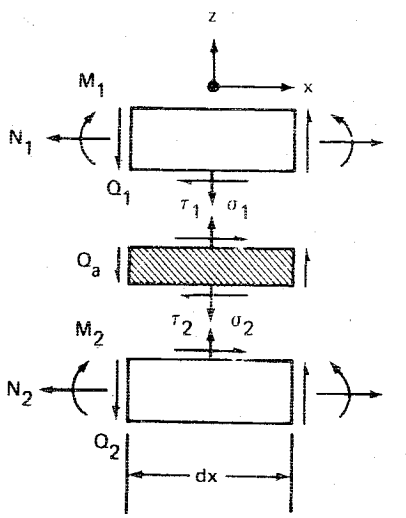

Fig. 2b Elements of typical joint including their interaction stresses.

moment and horizontal force resultants as

$$\bar{u}_1' = \frac{1}{E^* t}\left(N_1 + 6\frac{M_1}{t}\right) \tag{9a}$$

and

$$\bar{u}_2' = \frac{1}{E^* t}\left(N_2 - 6\frac{M_2}{t}\right) \tag{9b}$$

Following Assumption 3 and imposing compatibility of the bond with the upper and lower adherends, the adhesive displacements are given by

$$w_a(x,z) = \frac{w_1 + w_2}{2} + \frac{z}{h}(w_1 - w_2) \tag{10a}$$

and

$$u_a(x,z) = \frac{\bar{u}_1 + \bar{u}_2}{2} + \frac{z}{h}(\bar{u}_1 - \bar{u}_2) \tag{10b}$$

where the w_i and $\bar{u}_i$ (see Fig. 3) are functions of x only.

Substituting derivatives of Eq. (10) into the complete adhesive shear-strain/displacement equation

$$\gamma_a = \frac{\partial u}{\partial z} + \frac{\partial w}{\partial x} \tag{11}$$

and the shear elastic stress-strain law, yields

$$\tau_i = G_a\left(\frac{\bar{u}_1 - \bar{u}_2}{h} + w_i'\right) \quad i = 1,2 \tag{12}$$

The term w_i' in Eq. (12) has been neglected by previous investigators and constitutes the term from which most of the differences introduced in the present work originate.

Combining Eqs. (7) and (12), the average shear stress, τ_0, is given by

$$\tau_0 = \tau(z=0) = \frac{\bar{u}_1 - \bar{u}_2}{h} + \frac{w_1' + w_2'}{2} \tag{13}$$

and substitution of Eqs. (8) and (9) into the derivative of Eq. (13) yields

$$\tau_0' = \frac{G_a}{E^* th}\left[N_1 - N_2 + 6(1+\beta)\frac{M_1 + M_2}{t}\right] \tag{14}$$

where

$$\beta \equiv h/t \tag{15}$$

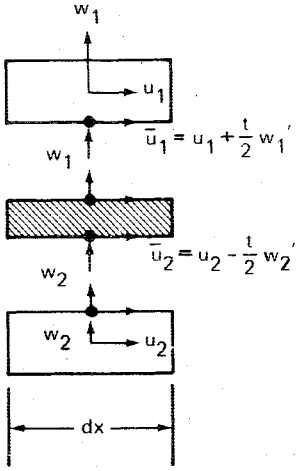

Fig. 3 Deflection sign convention for adhesive and adherends.

Differentiating Eq. (14) and substitutions in Eqs. (3), (5), and (7) yields

$$\tau_0'' = \frac{G_a}{E^* th}\left[2(1+3[1+\beta]^2)\tau_0 - \frac{6(1+\beta)}{t}(Q_1 + Q_2 + Q_a)\right] \tag{16}$$

Differentiating again and making use of Eq. (2), we finally obtain the governing adhesive shear stress differential equation

$$\tau_0''' - 2(\lambda/c)^2(1+3[1+\beta]^2)\tau_0' = 0 \tag{17}$$

where

$$\lambda^2 \equiv \frac{G_a c^2}{E^* th} \tag{18}$$

To obtain a corresponding equation for the adhesive peel stress, σ_a, we next write the stress-strain law for the bond material assuming Poisson's ratio is zero. Therefore,

$$\sigma_a = E_a \frac{\partial w}{\partial z} \tag{19}$$

which combines with Eq. (13) to give

$$\sigma_a = E_a(w_1 - w_2)/h \tag{20}$$

Thus, under Assumption 2, the adhesive peel stress does not vary with the thickness coordinate as does the shear stress, i.e.,

$$\sigma_1 = \sigma_2 = \sigma_a \tag{21}$$

Differentiating Eq. (20) thrice and introducing Eq. (8) and then Eq. (3), we obtain

$$\sigma_a''' = \frac{12E_a}{E^* t^3 h}\left([\tau_1 - \tau_2]\frac{t}{2} - Q_1 + Q_2\right) \tag{22}$$

From Eqs. (12) and (20) we note that

$$\tau_1 - \tau_2 = G_a(w_1' - w_2') = \frac{G_a h}{E_a}\sigma_a' \tag{23}$$

Therefore, Eq. (22) becomes

$$\sigma_a''' = \frac{12E_a}{E^* t^3 h}\left(\frac{G_a ht}{2E_a}\sigma_a' - Q_1 + Q_2\right) \tag{24}$$

Differentiating Eq. (24) once again and employing Eqs. (4) and (21), we finally obtain

$$\sigma_a^{iv} - \frac{6\beta\lambda^2}{c^2}\sigma_a'' + \frac{\rho^2}{c^4}\sigma_a = 0 \tag{25}$$

where

$$\rho^2 \equiv \frac{24E_a c^4}{E^* ht^3} \tag{26}$$

Although the governing adhesive peel and average shear stress differential equations, Eqs. (25) and (17), respectively, are uncoupled from one another, the shear stress components τ_1 and τ_2 are related to σ_a. This may be seen by combining Eqs. (13) and (23) to obtain

$$\tau_1 = \tau_0 + \Delta\tau \tag{27a}$$

and

$$\tau_2 = \tau_0 - \Delta\tau \tag{27b}$$

where

$$\Delta\tau = \frac{G_a h}{2E_a}\sigma_a' \tag{27c}$$

It may be noted at this point that the adhesive displacement field, based upon Assumption 3, introduces an inconsistency in the vertical equilibrium of the bond layer. This may be seen from Fig. 2b and Eqs. (2), (4), and (21) which indicate that,

$$Q_a' = \sigma_2 - \sigma_1 \tag{28a}$$

and

$$\sigma_2 - \sigma_1 = 0 \tag{28b}$$

while Eq. (6) yields

$$Q_a' = h\tau_0' \tag{28c}$$

Now, since τ_0 is not constant, Eqs. (28a-c) are inconsistent. In the results which follow, Eqs. (28b) and (28c) are satisfied, but Eq. (28a) is violated.

Boundary Conditions

The internal adherend loads at the ends of the joint (see Fig. 4) are

$$M_1 = M_0, \quad N_1 = N_0, \quad Q_1 = Q_0 \tag{29a}$$

$$M_2 = 0, \quad N_2 = 0, \quad Q_2 = 0 \tag{29b}$$

at $x = c$, and

$$M_1 = 0, \quad N_1 = 0, \quad Q_1 = 0 \tag{29c}$$

$$M_2 = -M_0, \quad N_2 = N_0, \quad Q_2 = Q_0 \tag{29d}$$

at $x = -c$.

From Eq. (14) and the preceding relations, we obtain the boundary conditions on Eq. (17) as

$$\tau_0'(\pm c) = \pm\frac{G_a}{E^* th}\left[N_0 + \frac{6(1+\beta)}{t}M_0\right] \tag{30}$$

to which we must append the horizontal equilibrium condition for either adherend and the associated upper or lower half of the adhesive, i.e.,

$$\int_{-c}^{c} \tau_0 dx = N_0 \tag{31}$$

By Eqs. (24) and (28) we obtain

$$\sigma_a'''(\pm c) - \frac{6\beta\lambda^2}{c^2}\sigma_a'(\pm c) = \mp\frac{12E_a}{E^* t^3 h}Q_0 \tag{32}$$

and from Eqs. (8), (20), and (28)

$$\sigma_a''(\pm c) = \frac{12E_a}{E^* h t^3}M_0 \tag{33}$$

which are used, in conjunction with Eq. (25), to obtain a solution for the peel stress.

Although N_0, M_0, and Q_0 must be known in order to apply the boundary conditions, only one of these, N_0, is generally known and the others must be obtained from overall equilibrium and compatibility. A consideration of overall joint moment equilibrium (Fig. 4), shows that Q_0, N_0, and M_0 are related thusly:

$$2cQ_0 + 2M_0 = N_0(t+h) \tag{34}$$

or, employing Eq. (15)

$$\frac{Q_0}{N_0} = \frac{t}{2c}\left(1+\beta - \frac{2M_0}{N_0 t}\right) \tag{35}$$

Equation (35) supplies one of the dependencies between the edge loads. The second dependency is between M_0 and N_0 only, and is obtained as follows.

Upon application of a tensile load to a single-lap adhesive joint, edge moments, M_0, will develop to react the applied couple, $N_0 t\,(1+\beta)$, and the joint will rotate. This creates a geometric nonlinear effect which reduces the edge moment and introduces transverse shears at the ends of the joint. The ratio of the reduced moment to its linear (undeformed joint) counterpart is defined by a factor k, where

$$k = \frac{M_0}{(N_0 t/2)(1+\beta)} \tag{36}$$

Values of k were obtained by Goland and Reissner[1] through application of adherend compatibility at the ends of the overlap region. However, besides ignoring the β factor in Eq. (36), they neglected to include the effect of the adhesive when computing the bending stiffness in the joint overlap region. Thus, their analysis implied the physically unreasonable flexure stress distribution, at the ends of the joint region, shown in Fig. 5a. This was detected by Hart-Smith,[5] who refined their analysis in a clever manner. The result was the more realistic stress distribution at the ends of the joint as shown in Fig. 5b.

Comparison plots of k for both Refs. 1 and 5, as given by Hart-Smith, are reproduced here as Fig. 6. As can be seen, k depends upon the joint loading to stiffness ratio parameter, ξ, where

$$\xi c = \left[\frac{12N_0 c^2}{E^* t^3}\right]^{1/2} \tag{37}$$

It is recommended that Hart-Smith's k values be used as they are probably more accurate.

Nondimensionalization

Defining nondimensional shear stress, τ^*, peel stress, σ^*, and length coordinate, x^*, as

$$\tau^* \equiv \frac{\tau_0}{\bar{\tau}}, \quad \Delta\tau^* \equiv \frac{\Delta\tau}{\bar{\tau}}, \quad \sigma^* \equiv \frac{\sigma_a}{\bar{\tau}}, \quad x^* = \frac{x}{c} \tag{38a-d}$$

and average shear stress, $\bar{\tau}$,

$$\bar{\tau} \equiv N_0/2c \tag{38e}$$

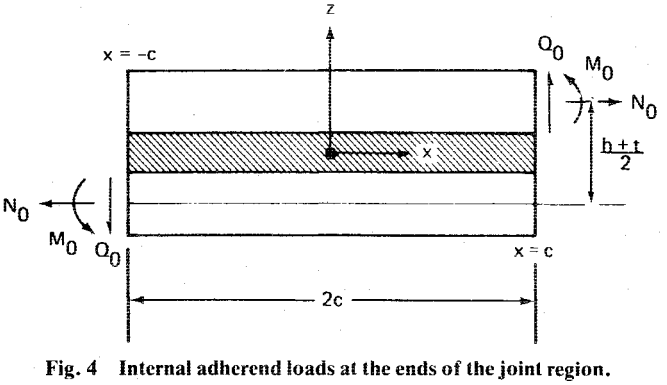

Fig. 4 Internal adherend loads at the ends of the joint region.

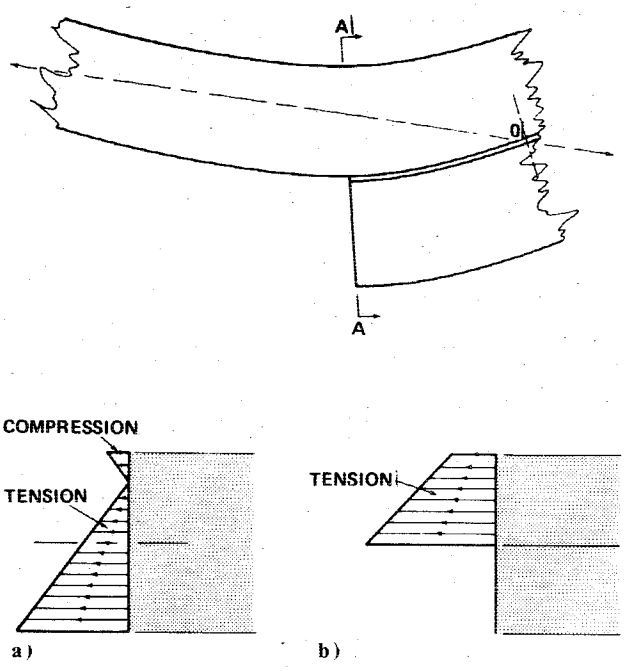

Fig. 5 Comparison of stress distribution at edge of joint (section A-A) as given by: a) Goland and Reissner and b) Hart-Smith.

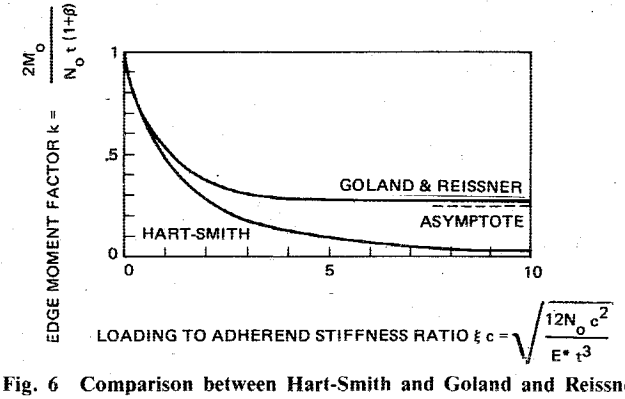

Fig. 6 Comparison between Hart-Smith and Goland and Reissner edge moment factor.

we obtain, from Eqs. (17), (30) and (31),

$$\tau^{*\prime\prime\prime} - 2\lambda^2(1+3[1+\beta]^2)\tau^{*\prime} = 0 \tag{39a}$$

$$\Delta\tau^* = \frac{hG_a}{2cE_a}\sigma^{*\prime} \tag{39b}$$

$$\tau^{*\prime}(\pm 1) = \pm 2\lambda^2[1+3(1+\beta)^2 k] \tag{40}$$

and

$$\int_{-1}^{1} \tau^* dx^* = 2 \tag{41}$$

where we have made use of Eq. (35) and a redefinition of the derivative term $(\,)'$, i.e.,

$$(\,)' \equiv \frac{d(\,)}{d(x/c)} = \frac{d(\,)}{dx^*} \tag{42}$$

Similarly, for Eqs. (25), (32), and (33), we obtain

$$\sigma^{*iv} - 6\beta\lambda^2\sigma^{*\prime\prime} + \rho^2\sigma^* = 0 \tag{43}$$

$$\sigma^{*\prime\prime\prime}(\pm 1) - 6\beta\lambda^2\sigma^{*\prime}(\pm 1) = \mp k\gamma\rho^2(1+\beta) \tag{44}$$

$$\sigma^{*\prime\prime}(\pm 1) = k\gamma\rho^2(1+\beta) \tag{45}$$

where use has been made of Eqs. (35), (36), (42), and the new dimensionless variable

$$\gamma \equiv t/2c \tag{46}$$

Since τ^* is the through-the-thickness average nondimensional stress, by virtue of Eqs. (27), (35), (38), and (39b), the maximum nondimensional stress at the bond/adherend interfaces is given by

$$\tau^{**} = \tau^* \pm \Delta\tau^* \tag{47}$$

The seven nondimensional governing equations are compared with their previous counterparts, as developed by Goland and Reissner[1] in Table 1.

Solutions

The solution to Eq. (39) for the nondimensional middle surface shear stress, τ^*, is

$$\tau^* = A\cosh\lambda\sqrt{2+6(1+\beta)^2}\,x^* + B \tag{48}$$

where the constants A and B are obtained from differentiation and integration of Eq. (48) and substitution into Eqs. (40) and (41).

The solution to Eq. (43) for the nondimensional peel stress, σ^*, is of the form

$$\sigma^* = C\sinh\alpha_1 x^*\sin\alpha_2 x^* + D\cosh\alpha_1 x^*\cos\alpha_2 x^* \tag{49}$$

where

$$\alpha_1^2 = \frac{3\beta\lambda^2}{2} + \frac{\rho}{2} \tag{50}$$

and

$$\alpha_2^2 = -\frac{3\beta\lambda^2}{2} + \frac{\rho}{2} \tag{51}$$

The constants C and D are obtained upon subsitution of the derivatives of Eq. (49) into Eqs. (44) and (45).

Typical results for τ^{**}, τ^*, and σ^* given by Eqs. (47-49), are compared with those obtained by Goland and Reissner's solutions in Figs. 7 and 8 for a typical set of parameters.

Maximum nondimensional shear and peel stress results, as determined by Eqs. (47-50), are presented in Figs. 9-13, respectively, for a range of parameters. Also shown are the corresponding solutions employing Goland and Reissner's equations.

Discussion

Through examination of Table 1 and Fig. 5, it is observed that the significant nondimensional joint parameters, which govern the stress parameters τ^*, $\Delta\tau^*$, and σ^*, are $(\xi c)^2$, the ratio of stretching load-level to adherend bending stiffness in the joint region, which governs k, the ratio of edge moment to applied load couple; λ^2, the adhesive shear to adherend stretching stiffness ratio; ρ^2, the adhesive peel to adherend bending stiffness ratio; and the geometric ratios β and γ.

Based upon the results of Figs. 7-13, a number of conclusions regarding the effect of bond thickness upon elastic adhesive stresses may be drawn:

1) Variation of shear stress through the bond thickness may be significant and only a theory which employs the complete shear-strain expression, such as the present one, can predict this effect (see Figs. 7 and 10).

Table 1 Comparison of adhesive stress equations with and without bond thickness effects

Equation	With bond thickness effects (present analysis)	Without bond thickness effects (Refs. 1 and 5)
Shear differential equation	$\tau^{*\prime\prime\prime} - 2\lambda^2(1+3[1+\beta]^2)\tau^* = 0$	$\tau^{*\prime\prime\prime} - 8\lambda^2\tau^{*\prime} = 0$
Shear boundary conditions	$\tau^{*\prime}(\pm 1) = \pm 2\lambda^2(1+3k[1+\beta]^2)$	$\tau^{*\prime}(\pm 1) = 2\lambda^2(1+3k[1+\beta])$
	$\int_{-1}^{+1} \tau^* dx^* = 2$	same
Maximum shear stress	$\tau^{**} = \tau^* \pm \Delta\tau^*$	$\tau^{**} = \tau^*$
Peel differential equation	$\sigma^{*iv} - 6\beta\lambda^2\sigma^{*\prime\prime} + \rho^2\sigma^* = 0$	$\sigma^{*iv} + \rho^2\sigma^* = 0$
Peel boundary conditions	$\sigma^{*\prime\prime} = \rho^2 k\gamma[1+\beta]$	same
	$\sigma^{*\prime\prime\prime} - 6\beta\lambda^2\sigma^{*\prime} = -\rho^2\gamma[1+\beta](1-k)$	same

Nondimensional variables

$$x^* = \frac{x}{c} \quad \tau^* = \frac{2\tau_0 c}{N_0} \quad \sigma^* = \frac{2\sigma_a c}{N_0} \quad \beta = \frac{h}{t} \quad \lambda^2 = \frac{G_a c^2}{E^* t h} \quad \rho^2 = \frac{24E_a c^4}{E^* h t^3} \quad \gamma = \frac{t}{2c} \quad k = \frac{2M_0}{N_0 t(1+\beta)}$$

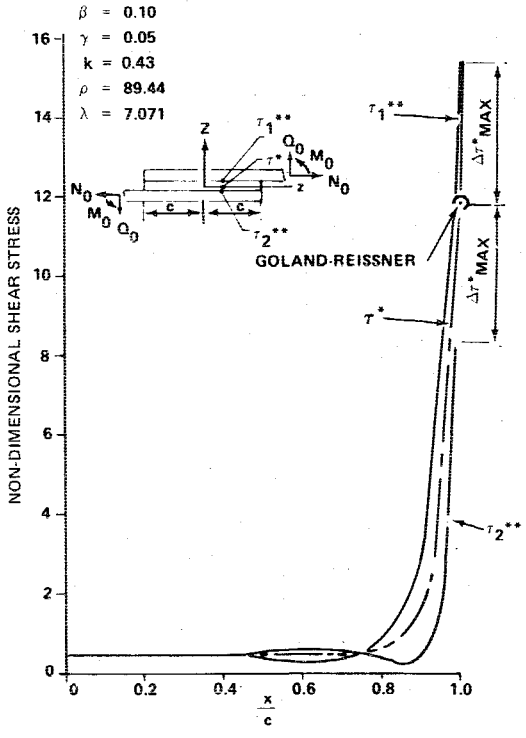

Fig. 7 Shear stress distribution.

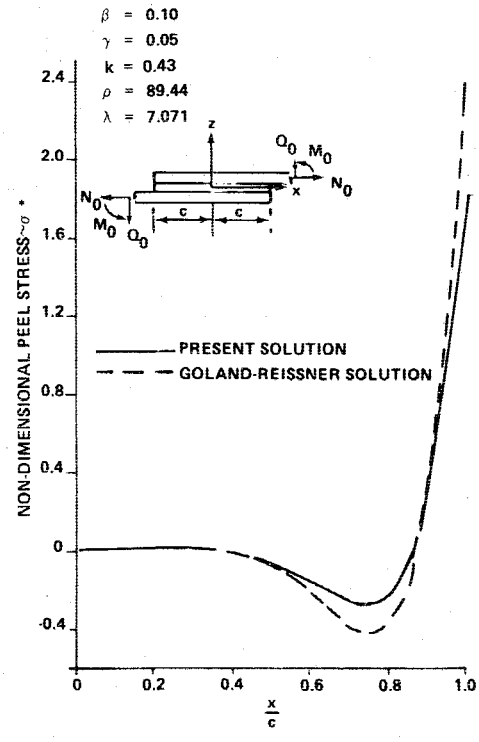

Fig. 8 Peel stress distribution.

2) The main difference in stresses obtained between theories which include and those which neglect bond thickness occur at the edges of the joint where the stresses are highest (see Figs. 7 and 8).

3) The shear and peel stress distributions may vary significantly between theories which include and those which ignore the effect of bond thickness (see Figs. 7-13).

4) The inclusion of bond thickness effects increases the predicted maximum shear stresses and reduces the predicted peel stresses (see Figs. 7-13).

5) Two separate terms combine to produce an increase in joint shear stress, τ^{**}. One is caused by the increase in β, which increases the middle surface shear stress, τ^*, and the second, $\Delta\tau^*$, depends upon λ^2 and ρ^2 as well (see Figs. 9 and 10).

6) The effect of bond thickness is more pronounced when the parameter λ is largest and the parameter ρ is smallest, i.e., joints with short overlaps, thick adherends, and stiff adhesives (see Figs. 9-13).

It should be noted that an adhesive stress failure is not the only mode that should be considered when predicting joint strength. Other important failure modes include adherend bending and, for composites, delamination. These types of failure are most likely to occur at joint edges, where the adherend bending and delamination stresses are highest. However, for joints in which adhesive failure is the common mode, we have observed from numerous tests, that bond failures occur consistently along the bond adherend interfaces, in the antisymmetrical pattern indicated in Figure 14. This is evidenced by the distribution of bond material which

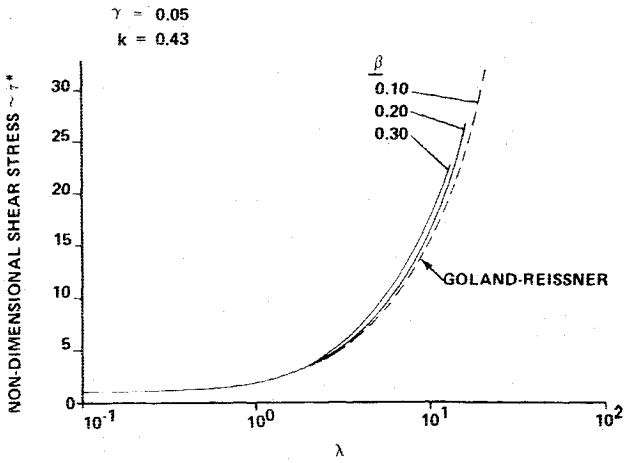

Fig. 9 Maximum middle surface shear stress.

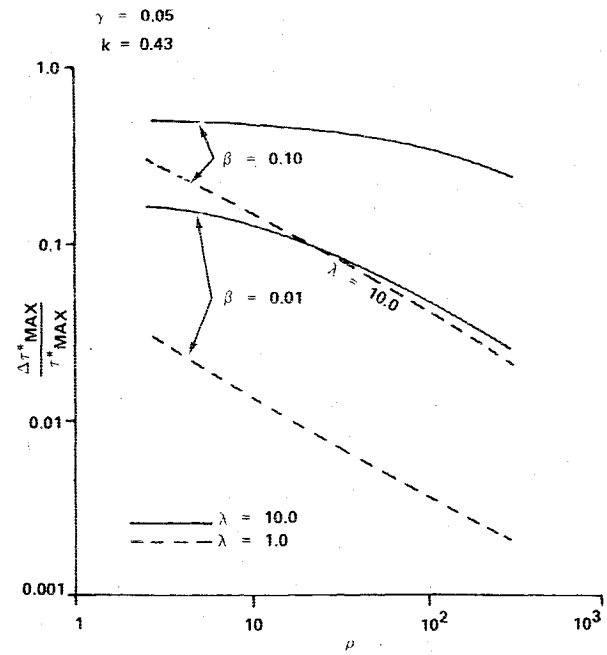

Fig. 10 Effect of bond thickness on maximum shear stress.

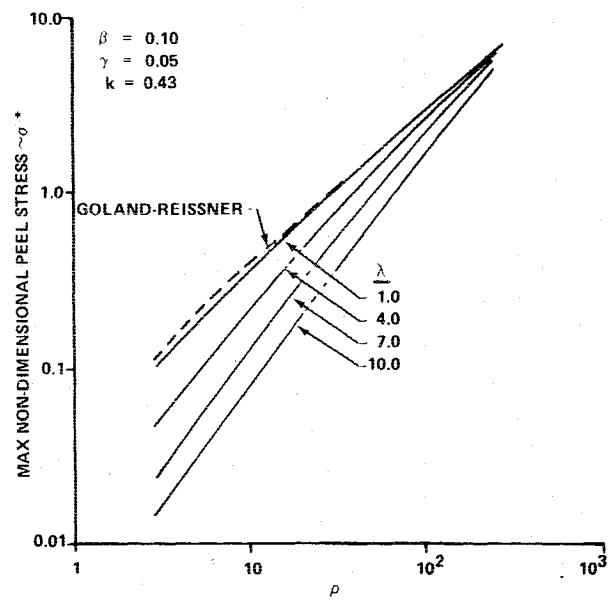

Fig. 11 Effect of varying λ on maxσ^* for $\beta = 0.10$.

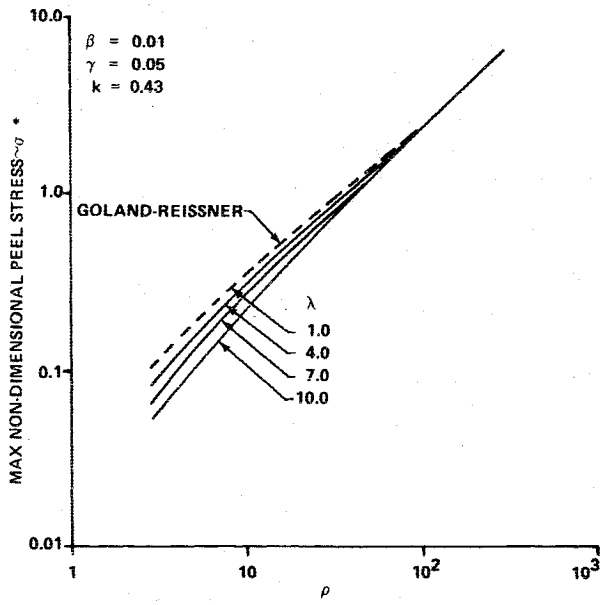

Fig. 12 Effect of varying λ on maxσ^* for $\beta = 0.01$.

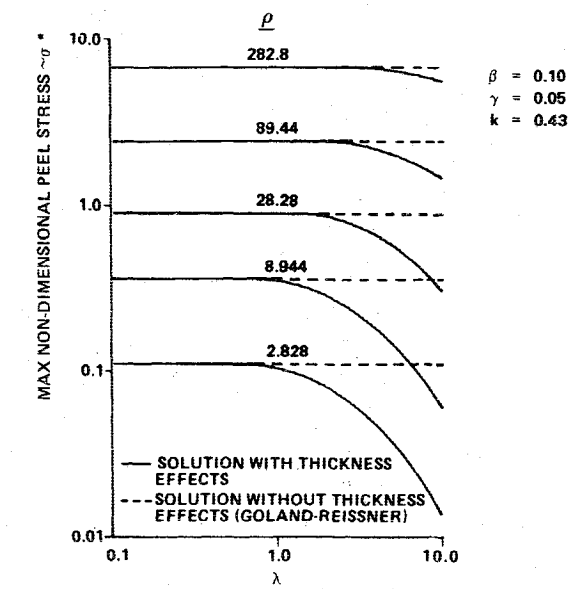

Fig. 13 Effect of varying λ on σ^*.

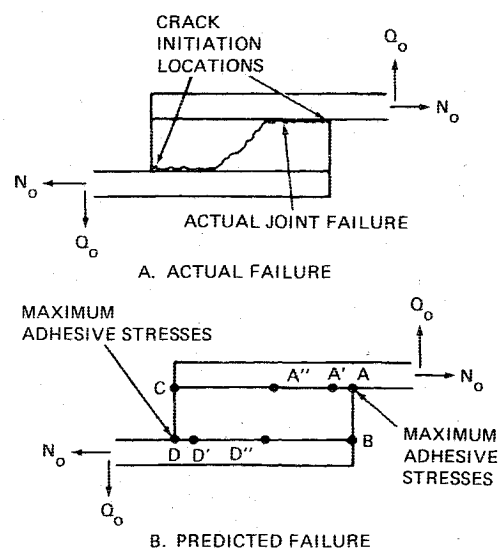

Fig. 14 Comparison of actual joint failures with points of maximum adhesive stresses.

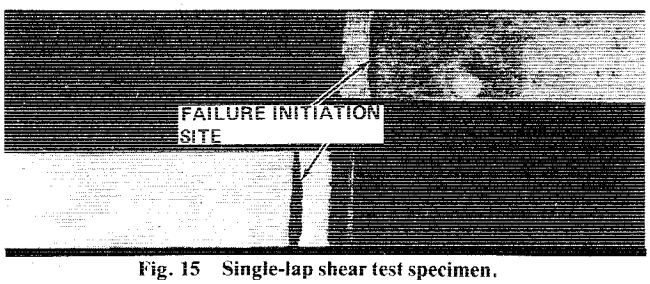

Fig. 15 Single-lap shear test specimen.

remains on both halves of the joint. This particular failure mode can be explained very nicely by the present theory as follows. Reasoning that the shear stress is highest at points A and D (see Fig. 14b), they represent logical points for cracks to originate at. As these cracks propagate, they create a shorter joint with even higher stresses at points A' and D'. Thus, the crack propagates in a castastrophic manner to points A'' and D'' where finally it jumps across the bond at the joint's origin.

Although it may be argued that higher order adherend theories[2-4] predict that peak shear stresses occur slightly behind the joint edges, we note that careful examination of the failed test specimens reveal a narrow band at the edges, A and D, to which some bond material has remained attached. This indicates a different type failure at the extreme edges which, in turn, implies a boundary-layer effect. To verify our joint-adhesive-failure hypothesis further, it remains to couple our through-the-thickness shear-stress-variation work with a higher order theory, and to compare the computed boundary-layer thicknesses with those observed in test.

Figure 15 presents a standard single-lap bonded joint test specimen that has been loaded to failure. The specimen failure was initiated at the location already described (see Fig. 14a). It is noted that there is a lip of adhesive remaining at the ends of the overlap region due to the low shear stresses there resulting from the already mentioned boundary layer effect and the fact that some adhesive squeezes out of the end of the overlap when the specimen is manufactured. The failure surface propagated from the initiation points to the center of the overlap region which is consistent with the theory presented.

Acknowledgment

The authors wish to acknowledge the partial support of this program by S. Dastin and J. Mahon of the Grumman Aerospace Corp., Advanced Development Group.

References

[1] Goland, M. and Reissner, E., "The Stresses in Cemented Joints," *Journal of Applied Mechanics*, Vol. 11, March 1944, pp. A17-A27.

[2] Grimes, G. C., et al., "The Development of Non-Linear Analysis Methods for Bonded Joints in Advanced Filamentary Composite Structures," AFFDL-TR-72-97, Sept. 1972.

[3] Dickson, J. N., Hsu, T. M., and McKinney, J. M., "Development of an Understanding of the Fatigue Phenomena of Bonded and Bolted Joints in Advanced Filamentary Composite Materials," Vol. 1, AFFDL-TR-72-64, June 1972.

[4] Renton, W. J. and Vinson, J. R., "The Analysis and Design of Anisotropic Bonded Joints," Univ. of Delaware, MAETR 171, Aug. 1974.

[5] Hart-Smith, L. J., "Adhesive-Bonded Single-Lap Joints," NASA CR-112236, Jan. 1973.

[6] Corvelli, N. and Saleme, E., "Analysis of Bonded Joints," Grumman Aerospace Corp., Rept. No. ADR 02-01-70.1, July 1970.